



Probing the cortical network underlying the psychological refractory period: A combined EEG–fMRI study

G. Hesselmann^{a,*}, G. Flandin^b, S. Dehaene^{c,d,e}

^a Department of Neurobiology, Weizmann Institute of Science, Rehovot, Israel

^b Wellcome Trust Centre for Neuroimaging at UCL, Institute of Neurology, University College London, London, UK

^c INSERM, Cognitive Neuroimaging Unit, Gif sur Yvette, France

^d CEA, I2BM, NeuroSpin center, Gif sur Yvette, France

^e Collège de France, Paris, France

ARTICLE INFO

Article history:

Received 25 January 2011

Revised 2 March 2011

Accepted 4 March 2011

Available online 11 March 2011

Keywords:

PRP

Dual-task

fMRI

EEG

P3

Combined EEG–fMRI

ABSTRACT

Human performance exhibits strong multi-tasking limitations in simple response time tasks. In the psychological refractory period (PRP) paradigm, where two tasks have to be performed in brief succession, central processing of the second task is delayed when the two tasks are performed at short time intervals. Here, we aimed to probe the cortical network underlying this postponement of central processing by simultaneously recording electroencephalography (EEG) and functional magnetic resonance imaging (fMRI) data while 12 subjects performed two simple number-comparison tasks. Behavioral data showed a significant slowing of response times to the second target stimulus at short stimulus-onset asynchronies, together with significant correlations between response times to the first and second target stimulus, i.e., the hallmarks of the PRP effect. The analysis of EEG data showed a significant delay of the post-perceptual P3 component evoked by the second target, which was of similar magnitude as the effect on response times. fMRI data revealed an involvement of parietal and prefrontal regions in dual-task processing. The combined analysis of fMRI and EEG data—based on the trial-by-trial variability of the P3—revealed that BOLD signals in two bilateral regions in the inferior parietal lobe and precentral gyrus significantly covaried with P3 related activity. Our results show that combining neuroimaging methods of high spatial and temporal resolutions can help to identify cortical regions underlying the central bottleneck of information processing, and strengthen the conclusion that fronto-parietal cortical regions participate in a distributed “global neuronal workspace” system that underlies the generation of the P3 component and may be one of the key cerebral underpinnings of the PRP bottleneck.

© 2011 Elsevier Inc. All rights reserved.

Introduction

Despite the primate brain's massively distributed processing architecture (Felleman and Van Essen, 1991), reminiscent of the multiple-processor design of parallel computers (Nelson and Bower, 1990), human performance exhibits surprisingly strong limitations in multi-tasking. In one of the simplest multi-tasking experiments (Fig. 1), two target stimuli (T1 and T2, e.g., two tones) are presented in brief succession, and subjects' responses (R1, R2) to both targets are recorded. Under these simple dual-task conditions, response times to the second stimulus (RT2) show a significant increase when the stimulus-onset asynchrony (SOA) between the two tasks is shortened; response times to the first stimulus (RT1), however, remain largely unaffected by SOA. This classic and widely replicated finding

has been dubbed the “psychological refractory period” (PRP), in analogy to post-stimulation refractory phenomena observed in nerves (Telford, 1931). The original hypothesis put forward to explain it was that the “central organizing times” of stimulus processing cannot overlap for two stimuli, and thus have to unfold strictly serially, one after the other (Welford, 1952). This notion of non-overlapping “organizing times”, or in other words, a serial processing stage that acts as a bottleneck of information processing, remains a central ingredient of modern theories of the PRP. The central bottleneck model (Pashler, 1994, 1998), which emerged from numerous behavioral experiments, involves three stages of processing: a perceptual (P), a central (C), and a motor (M) stage. According to the model, P and M stages can occur in parallel, while the C stages of two tasks cannot overlap and have to be processed serially. Thus, at short SOAs, central processing for T2 is deferred, or passively queued, until central processing for T1 is completed, and RT2 is increased (Fig. 1).

Various behavioral experiments have associated the central processing stage to response selection, i.e., the mapping between sensory information and motor action (De Jong, 1993; Pashler and

* Corresponding author at: Department of Neurobiology, Weizmann Institute of Science, 76100 Rehovot, Israel. Fax: +972 8 934 4140.

E-mail address: g.hesselmann@gmail.com (G. Hesselmann).

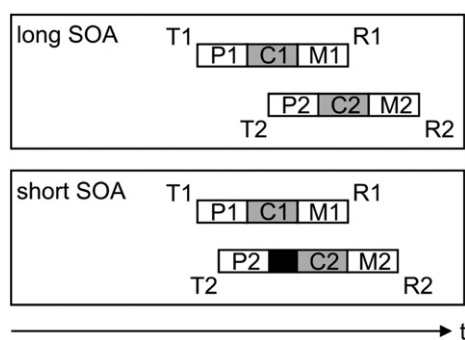


Fig. 1. Central bottleneck model of the psychological refractory period (PRP) in overlapping dual-task paradigms. Two targets (T1, T2) are presented with variable stimulus-onset asynchrony (SOA). The PRP refers to the increase of response time for the second-task response (R2) when the SOA is shortened; response time for the first-task response (R1) is largely unaffected by SOA. According to the central bottleneck model, target processing involves a perceptual (P), a central (C), and a motor (M) stage. P and M stages can occur in parallel. Central stages of two tasks cannot overlap and have to be processed serially; at short SOAs, central processing for T2 is deferred (black box) until central processing for T1 is completed.

Johnston, 1989). Recently, it has been proposed that the C stage can be characterized as a decision-making process based on the noisy integration of evidence (Sigman and Dehaene, 2005). Alternative models argue against a structural bottleneck of stimulus processing, which invariably results in passive queuing of the second stimulus, and instead propose a strong influence of executive control in the strategic monitoring of the two tasks (Logan and Gordon, 2001; Meyer and Kieras, 1997a,b), or the ability to share processing capacity between them (Navon and Miller, 2002; Tombu and Jolicoeur, 2003). According to shared capacity models, response selection can occur in parallel, but with limited processing resources differentially weighted for one task over the other, resulting in a lag between RT1 and RT2 typical for the PRP. Several dual-task studies have reported behavioral congruency effects that poses a major challenge for the bottleneck model, namely the dependence of RT1 on the response that is required for the second stimulus, referred to as *backward crosstalk* (as opposed to crosstalk from T1 on RT2). Backward crosstalk effects, which are observed when both tasks are similar [(Logan and Delheimer, 2001; Logan and Schulkind, 2000), but see (Miller, 2006)], are difficult to reconcile with the strictly serial bottleneck model, because they provide evidence that central processing for T2 may start before the C stage for T1 is complete.

To further describe and anatomically locate the cognitive processes underlying the PRP, a rich body of evidence, including data from studies using event-related potentials (ERPs), functional magnetic resonance imaging (fMRI), and recently computational modeling (Zylberberg et al., 2010), has been accumulated. Studies using fMRI have reported various frontal and parietal regions associated with the PRP (Marois and Ivanoff, 2005), but the results do not appear to converge and strongly depend on the statistical approaches used to test for dual-task-specific effects (Szameitat et al., 2011). Isolating PRP related activity by contrasting dual-task against single-task activity, or alternatively, short SOA against long SOA trials, has highlighted different sets of regions in the lateral frontal, medial frontal, premotor and parietal cerebral cortex. Recently, studies using time-resolved fMRI have reported delayed peaks of activation in the left posterior lateral prefrontal cortex associated with the PRP (Dux et al., 2006), and PRP related temporal variations of activity in the bilateral parietal and frontal regions, respectively (Sigman and Dehaene, 2008). However, the sensitivity and interpretation of these studies also suffers from the low temporal resolution of fMRI.

A number of ERP studies investigating the PRP effect have targeted the amplitude and latency of the P3 (or, P300) component, which is characterized by a positive deflection broadly distributed over the

scalp, but with a focus over parietal electrodes (Picton, 1992; Sutton et al., 1965). Recently, it has been proposed that the P3, which has been linked to post-perceptual processes such as the context-updating of working memory (Coles et al., 1985; Donchin and Coles, 1988; Verleger et al., 2005), may be related to the access of a target stimulus to a global neuronal workspace associated with conscious report (Del Cul et al., 2007; Sergent et al., 2005). Based on the delay of the P3 evoked by the second target (T2-P3) some ERP studies have proposed an overlap between the cognitive processes mediating the PRP effect and P3-related processes (Dell'Acqua et al., 2005; Sigman and Dehaene, 2008), while the evidence from other studies, showing a large discrepancy between RT2 and T2-P3 latency modulations, suggests independent sources for PRP and P3 effects (Arnell et al., 2004; Luck, 1998). The latencies of earlier sensory ERP components, such as the P1 and N1, have been reported to remain stimulus-locked to both targets and show no postponement related to the PRP (Brisson and Jolicoeur, 2007; Sigman and Dehaene, 2008).

In the present study, our main aim was to probe the cortical network underlying the PRP by using a combination of simultaneously recorded high-temporal resolution EEG and high-spatial resolution fMRI responses. Due to recent advances in the combination of both neuroimaging methods (Herrmann and Debener, 2008; Laufs et al., 2008), fluctuations in EEG can be correlated to the simultaneously recorded fMRI data on a trial-by-trial basis, thus helping to identify the cerebral networks underlying dynamic changes in ERPs. Based on previous research (Dell'Acqua et al., 2005; Sigman and Dehaene, 2008) which showed a close link between the P3 component and the PRP, we hypothesized that the P3 would covary with the fMRI-BOLD signal in the dual-task situation of our PRP paradigm. By correlating the single-trial amplitudes of the P3 component with the single-trial blood-oxygen-level dependent (BOLD) fMRI signals, we were able to isolate a set of two bilateral homotopic regions in the precentral gyrus and inferior parietal lobe. The PRP paradigm used in our study consisted of two identical number-comparison tasks, thus allowing for an additional analysis of behavioral crosstalk effects (Logan and Delheimer, 2001; Logan and Schulkind, 2000).

Materials and methods

Participants

Fourteen male right-handed native French speakers participated in this study, which was conducted at the NeuroSpin neuroimaging center in the CEA campus of Saclay, France. Two subjects had to be excluded due to excessive head movements during the scans and strong residual noise in the EEG after preprocessing which rendered the identification of ERP component topographies impossible. All remaining twelve subjects (mean age 24, range 19 to 28 years) had normal or corrected-to-normal vision. All participants provided informed written consent to take part in the experiment.

Design and procedure

Subjects were asked to perform two number-comparison tasks ("smaller or larger than 5?") on two successive digits presented left or right of fixation. They received the clear instruction that they had to respond accurately and as fast as possible to each of them. Using Eprime software (Psychology Software Tools Inc., USA) target stimuli (numbers 1, 4, 6, or 9) were presented in white font ("Courier New") on a black background for 100 ms (Fig. 2). Stimuli were generated by an EIKI LC5000 projector with a refresh rate of 60 Hz, and projected from outside the scanner onto a screen placed at the end of the scanner's bore. The latency between trigger delivery and stimulus onset on the screen was measured offline before and after the experiment by means of the Black Box Toolkit (Black

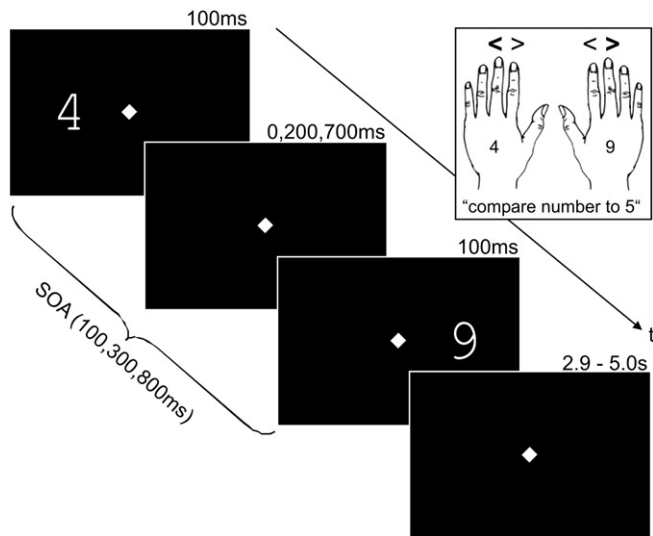


Fig. 2. Schematic illustration of the paradigm. In dual-task trials, two target numbers were presented on the screen for 100 ms, and subjects were instructed to perform two successive number-comparison tasks (“smaller or larger than 5?”). The stimulus onset asynchrony (SOA) between the first (T1) and the second target (T2) was varied between 100, 300, and 800 ms. Subjects responded to both targets with manual button presses. In two blocks of the dual-task condition, T1 was either presented on the left and T2 on the right (T1L–T2R block), or T1 was presented on the right and T2 on the left (T1R–T2L). In the single-task condition, only T1 was presented, in two blocks with T1 either left (T1L) or right of fixation (T1R).

Box Toolkit Ltd., UK) including a photodiode on the screen. The measured latency was constant at 2 refresh frames (33 ms), a value which was used to correct ERP recordings. The stimulus onset asynchrony (SOA) between the first (T1) and the second target (T2) was varied between 100, 300, and 800 ms. Based on psychophysical pilot experiments, the size and eccentricity of the target stimuli were carefully chosen so that subjects could perform the number comparison task while maintaining fixation. Target stimuli covered $1.7 \times 2.9^\circ$, and were video-projected at a viewing distance of 120 cm. Targets were presented either 3.0° left or right of a diamond-shaped fixation point (0.5°). Subjects responded to both targets with button presses, with the left hand to left targets, and with the right hand to right targets. For left targets, the middle finger served for responses to numbers smaller than 5, the index finger for numbers larger than 5; for right targets, the index finger served for responses to numbers smaller than 5, the middle finger for numbers larger than 5 (see inset of Fig. 2; in the example, the first number is 4, the second number is 9). Subjects were instructed to respond to both target numbers according to the order of their appearance. No error feedback was given.

In the dual-task condition, subjects performed two blocks of 144 trials (48 trials per SOA). Care was taken that all possible combinations of target numbers (T1, T2) were approximately balanced for each SOA (quasi-randomization). In one block, T1 was presented on the left and T2 on the right (T1L–T2R). In another block, T1 was presented on the right and T2 on the left (T1R–T2L). In each block, additional 48 trials were blank trials (“null trials”) without target stimuli. The length of a trial was jittered between 3.8 and 5.2 s in 0.2 s steps (mean: 4.5 s), and subjects could respond within that period. The order of trials was randomized in each block (approx. 15 min). In the single-task condition, only T1 was presented, in two blocks with T1 either left (T1L) or right of fixation (T1R). In the single-task blocks, 48 trials plus 16 blank trials were presented (approx. 5 min). The order of all four experimental blocks was randomized for each subject. Before the main experiment, subjects were extensively trained on the task (approx. 25 min) during the preparation of the EEG cap and electrodes.

Behavioral data analysis

Response times to the first (RT1) and second target (RT2) were determined separately for each subject and condition. Dual-task trials were divided into congruent (both target numbers smaller or larger than 5) and incongruent trials. Trials with RT1 or RT2 outliers (i.e., response times faster than the first quartile minus 1.5 times the inter-quartile range, or slower than the third quartile plus 1.5 times the inter-quartile range) were excluded from all further analysis. Separately for the first (R1) and second response (R2), response times were submitted to a 3×2 repeated measures ANOVA with factors “SOA” and “congruency”; response accuracies for R1 and R2 were submitted to a 3×2 repeated measures ANOVA with factors “SOA” and “response”. Degrees of freedom were Greenhouse–Geisser corrected (Greenhouse and Geisser, 1959) to account for possible violations of sphericity.

EEG acquisition

Continuous EEG recordings were acquired from 64 channels using two 32-channel MRI-compatible BrainAmp MR (BrainProducts, Germany) EEG amplifiers and the BrainCap64 MR electrode cap (EasyCap, Germany) with sintered Ag/AgCl ring electrodes; the last five subjects were recorded using a BrainCap64 MR with smaller pin electrodes. Sixty-two EEG electrodes were placed on the scalp according to a customized 10–20 system. The reference electrode was positioned between Fz and Cz in correspondence of the FCz electrode. The ground electrode was placed 1 cm inferior of Oz. Two additional electrodes were dedicated to the acquisition of the electrocardiogram (ECG) and electrooculogram (EOG). The ECG electrode was placed on the back of the subject, approx. 15 cm below the shoulder and approx. 3 cm left of the midline. The (vertical) EOG electrode was placed below the left eye. Electrode impedances were kept close to 5 k Ω by means of a mildly abrasive electrolyte paste (Abralylt 2000, EasyCap). The resolution and dynamic range of the EEG system were 0.5 μ V per bit and ± 16 mV, respectively. EEG was sampled at 5 kHz and bandpass-filtered online between 0.016 and 250 Hz. To synchronize the sampling clocks of the MR and EEG systems (Mandelkow et al., 2006) we used the SyncBox (BrainProducts), thus making the times of fMRI volume acquisition available for later gradient artifact removal. To further reduce broadband artifacts, the magnet’s helium pump was shut off during the time of EEG recording. We placed the EEG amplifiers and the battery (PowerPack, BrainProducts) outside of the magnet’s bore (approx. 1 m distance between EEG cap connectors and the amplifiers), aligned with the b0 field. EEG was recorded using the BrainRecorder software (Version 1.03, BrainProducts).

EEG preprocessing

BrainVision Analyzer software (Version 1.05, BrainProducts) was used for off-line correction of gradient artifacts (Allen et al., 2000; Becker et al., 2005). An artifact template based on a moving average of 15 gradient artifacts was subtracted from each artifact interval. Next, the EEG was downsampled to 250 Hz, low-pass filtered at 40 Hz, and exported to EEGLAB 6.03b (Delorme and Makeig, 2004) running on Matlab 7.1 R14 (The Mathworks, Inc.) for all further preprocessing and analysis. Pulse artifacts were removed using optimal basis sets (OBS) of principal components for the creation of artifact templates (Vanderperren et al., 2010), as implemented in the FMRIB plug-in for EEGLAB (Iannetti et al., 2005; Niazy et al., 2005). Care was taken that the pulse removal algorithm was restricted to clean, gradient-free EEG, i.e., badly corrected gradient artifacts typically at the beginning and the end of each EEG session were cut out before the correction. Before and after pulse artifact removal, we visually inspected the ERP images of all ECG and EEG traces time-locked to the onsets of pulse

artifacts as identified by the algorithm. If necessary, the onset of the pulse artifact was manually shifted to cover the true onset of the artifact (this was the case in three subjects). Next, the EEG was high-pass filtered at 0.5 Hz to remove slow drifts (Mantini et al., 2009; Mars et al., 2008; Strobel et al., 2008), epoched (−0.2 to 1.6 s, time-locked to T1 onset), and re-referenced to average reference. We rejected epochs with voltages exceeding $\pm 125 \mu\text{V}$, or transients exceeding $\pm 100 \mu\text{V}$. Between 2 and 16 of the total of 384 trials were rejected across subjects (mean: 8.0). Finally, independent-component analysis (ICA) was performed on the concatenated single-trial EEG data, separately for each experimental block, using the extended INFOMAX algorithm as implemented in EEGLab (Bell and Sejnowski, 1995). Each of the 4×62 ICs per subject was deconvoluted with an eye blink template of 400 ms, and ICs related to the eye blink were removed. The template was based on eye blinks in the raw EOG data which were identified, segmented and averaged using the Fieldtrip toolbox for EEG/MEG-analysis (Donders Institute for Brain, Cognition and Behaviour, Nijmegen, The Netherlands). Additionally, ICs manually classified as residual gradient noise were removed. Between 2 and 14 ICs per experimental block were removed across subjects (mean: 7.5).

EEG analysis

Our goal was to extract the amplitudes of the events associated with sensory (N1 components) and decision (P3 component) stages of T1 and T2 processing on every single trial, in order to cross-correlate these parameters with the BOLD signal from fMRI. To this aim, we combined the multiple linear regression method described by Sigman and Dehaene (2008) with a single-trial temporal template method similar to the one described by Quiroga and Garcia (2003). This method has two main features: first, it allows for a robust decomposition of the EEG signal into ERP components and, at the same time, delivers a quantification of their latencies (Sigman and Dehaene, 2008); second, it provides additional denoising of the EEG signal thus allowing for an estimation of trial-by-trial fluctuations in the evoked potentials. In our study, by defining templates on single-task trials, and regressing them to dual-task data, this method allowed us to quantify to what extent activations comparable to the single-task were present in the dual-task context.

First, we defined spatio-temporal templates which were designed to capture the temporal and scalp distribution characteristics of the N1 and P3. The spatio-temporal templates are based on the grand average EEG data. Two templates were used for the N1 component evoked by left and right single targets (T1), respectively (T1L-N1, and T1R-N1). A single template was used for the P3 evoked by both left and right single targets (T1-P3). Estimation of the onsets of the N1 and P3 components was based on the time course of the global field power, GFP (Lehmann and Skrandies, 1980). As can be seen in Fig. 4A, a first GFP peak occurred at approx. 200 ms, and a second broader GFP maximum started at approx. 400 ms. The corresponding ERP topographies at 200 ms revealed the occipital negativity of the lateralised T1L-N1 and T1R-N1 components. The ERP topography at 400 ms revealed the parietal positivity of the T1-P3 (more precisely, T1-P3b). Supplementary Fig. S1 shows the extracted spatio-temporal templates which were defined as the product of a spatial distribution of voltage over electrodes and a temporal profile of activation. The spatio-temporal distributions were extracted from the EEG data based on the corresponding peaks, as follows: for the N1, we used the voltages in a 100 ms window centered on 200 ms after the single target onset, thus from 150 to 250 ms—in agreement with prior research showing a sudden divergence of ERPs towards a later, non-perceptual stage after ~270 ms (Del Cul et al., 2007; Sergent et al., 2005); similarly, for the P3, we used the voltages in a 200 ms window centered on 400 ms (i.e., from 300 to 500 ms after single target onset), thus non-overlapping with the N1 time window. We chose a longer template for the P3 to account for the broader maximum of this

component. Finally, the templates were convolved with a temporal profile (cosine window) to accentuate the center of the template windows ($-\cos(2 * \pi * 10 * x)$ for N1, $-\cos(2 * \pi * 5 * x)$ for P3).

For each time point of the EEG, we then used a multiple linear regression procedure on sliding windows of data to extract the single-trial temporal profiles of the three spatio-temporal components. The center of the sliding window was successively moved from T1 onset to 1500 ms after T1 onset in all dual-task (i.e., dual-target) trials. At each time point, we extracted a window of EEG data centered on this time point, treated it as a long vector (of length = n electrodes \times m time points) and applied a multiple linear regression with the three previously defined spatio-temporal templates (note that no additional constant was needed because the data was average-referenced and therefore the voltages always averaged to zero). For the N1, the length of the extracted time window was 100 ms (25 time points at 250 Hz), and the length of the corresponding data vector was 1550 (62 electrodes \times 25 time points). For the P3, the length of the extracted time window was 200 ms (50 time points at 250 Hz), and the length of the corresponding data vector was 3100 (62 electrodes \times 50 time points). The resulting beta weights of this regression were taken as a measure of the instantaneous degree of activation of the corresponding ERP components. More specifically, high P3-related beta weights, for a given time point, indicate a good fit between the EEG data and the spatio-temporal P3 template within the corresponding time window. Hypothetically, identical P3 beta values are obtained if, for instance, 31 left-hemispheric electrodes show a good match, while 31 right-hemispheric electrodes do not (and vice versa); similarly, identical beta values are obtained if the match for the first 100 ms is good, while the match for the second 100 ms is not (and vice versa). The strength of using spatio-temporal templates, however, is that the match between data and templates has to be in spatial topography *and* in time.

Applying this procedure to extract single-trial data was challenging, given the intrinsic variability in single-trial EEG data. We took advantage of knowing the timing of the expected N1 and P3 activations. The index of N1 activation was taken as the mean beta for the corresponding N1 over a narrow time window of ± 24 ms around the expected peak time of 200 ms after the corresponding target (i.e., T1-N1 and T2-N1). The index of T1-P3 activation was taken as the mean beta of the P3 template over a wider time window of ± 48 ms around the expected peak time of 400 ms. For dual-task trials, we also extracted a second P3 (T2-P3), based on the results showing that T2 does elicit such secondary waveforms. At the single trial level, we restricted the analysis to the estimation of amplitudes (i.e., beta weights). In this way, we obtained, for each trial, a peak amplitude value for each of the three components. A standard subtraction method was applied to separate T2-P3 from T1-P3 related activity (Luck et al., 2000). Latencies of the T2-P3 component were estimated by finding—for each subject, but averaged across trials—the maximum beta weights in a predefined time window, ranging from T2 onset to 1500 ms after T1 onset.

fMRI acquisition and preprocessing

Functional blood oxygen level dependent (BOLD) images were acquired by T2*-weighted gradient-echo echo-planar imaging (33 slices, TR = 2000 ms, TE = 30 ms, flip angle = 87° , voxel size $3 \times 3 \times 3$ mm, inter-slice gap 10%) on a 3 T MRI scanner (Tim Trio, Siemens, Erlangen). In single-task blocks, we recorded 145 volumes per block. In dual-task blocks, we recorded 435 volumes per block. Anatomical images were acquired using a T1-weighted MPRAGE sequence (160 slices, TR = 2300 ms, TE = 2.98 ms, flip angle = 9° , FOV 256, voxel size $1.0 \times 1.0 \times 1.1$ mm). We used statistical parametric mapping (SPM5, Wellcome Trust Centre for Neuroimaging, London, UK) for image preprocessing (standard realignment, coregistration, normalization to MNI stereotactic space using unified segmentation,

spatial smoothing with a 6 and 12 mm full-width at half-maximum (FWHM) isotropic Gaussian kernel for single-subject and group analyses, respectively) and estimation of general linear models (GLMs) with a high-pass filter of 1/128 Hz and six rigid-body realignment parameters as nuisance covariates.

fMRI analysis: statistical parametric maps

BOLD-fMRI is largely insensitive to fast temporal events, although subtle phase analyses of single-event designs have shown to capture activation latencies on a 200 ms time scale (Sigman et al., 2007). Here, we used a fast event-related design inappropriate for this type of phase analysis. Therefore, regressors for event-related analysis were obtained by convolving each condition's impulse time series with a canonical hemodynamic response function without derivatives. To model single-task and dual-task activation in all trials, the statistical model included eight regressors: "T1L", "T1R", "T1L-T2R-SOA100", "T1L-T2R-SOA300", "T1L-T2R-SOA800", "T1R-T2L-SOA100", "T1R-T2L-SOA300", and "T1R-T2L-SOA800". The onset of each regressor was arbitrarily placed at T1 onset, and the onset of T2 was not modeled separately. For each subject, we estimated condition-specific effects and statistical parametric maps (SPMs) using a general linear model (GLM) approach (Friston et al., 1994), then created contrast images and entered these into second-level one-sample *t* tests. The following contrasts were calculated: "single-task>baseline", "dual-task>baseline", "dual task>mean of single tasks", "dual task>sum of single tasks", and "SOA 100>SOA 800". Unless otherwise stated, we report activations of this standard GLM analysis at $p < .05$ corrected at the cluster level for multiple comparisons using an auxiliary (uncorrected) voxel threshold of $p < .001$. This auxiliary threshold defines the spatial extent of activated clusters, which form the basis of our (corrected) inference. Group results are mapped onto the lateral and medial aspects of an inflated cortical surface of a canonical average brain as provided by SPM8 (Wellcome Trust Centre for Neuroimaging, London, UK). Anatomic labeling of cluster peaks was performed using the SPM Anatomy Toolbox Version 1.7b (Eickhoff et al., 2005). Parameter estimates in regions of interest were calculated using the MarsBaR Toolbox Version 0.42 for SPM (Brett et al., 2002).

fMRI correlates of trial-by-trial ERP variability

As described above, we treated each fMRI trial, even when it comprised two successive targets as a single and temporally unresolved hemodynamic event whose onset was placed at T1 onset. In the EEG-informed fMRI analysis, our goal was to use the simultaneous EEG measure as a predictor of the amplitude of this single-trial hemodynamic response (Debener et al., 2006), in order to identify cortical regions whose BOLD signal correlated with the extracted ERP components. The first analysis aimed to identify regions where fMRI activation covaried with the peak amplitudes of the T1-P3 and T2-P3, respectively. We modeled each dual-task trial (i.e., "T1L-T2R-SOA100", "T1L-T2R-SOA300", "T1L-T2R-SOA800", "T1R-T2L-SOA100", "T1R-T2L-SOA300", and "T1R-T2L-SOA800") by a sum of five hemodynamic functions without derivatives: the event onset regressor, and four (T1-N1, T2-N1, T1-P3, T2-P3) parametric modulators to achieve a complete model of EEG responses in each trial. The parametric modulators, based on the trial-by-trial amplitudes (beta values) of the corresponding ERP components (Fig. 5A), were serially orthogonalized in the order listed above (Friston et al., 2007). After general linear model estimation, we created two contrast images, "T1-P3 parametric modulator>baseline", and "T2-P3 parametric modulator>baseline", for each subject and entered these into second-level one-sample *t* tests to create whole-brain SPMs.

In the second approach, we restricted the EEG-informed fMRI analysis to a number of regions of interest (ROIs). These regions were

identified based on the contrasts "dual-task>mean of single-tasks", "dual-task>sum of single-tasks", and "SOA 100>SOA 800" (Fig. 6). We limited the ROIs to the significant cortical peaks listed in Table 1, excluding area right MT which most likely responded to apparent motion ("phi phenomenon") in dual-task trials (see fMRI results). For each ROI, we operationalized single-trial BOLD activity by the average parameter estimate across all voxels within a spherical volume of 6 mm in diameter, centered on the corresponding peak location (based on the group maps). Because the single-trial peak amplitudes for the T1-P3 and T2-P3 components were significantly correlated (see EEG results), we combined T1-P3 and T2-P3 beta values to a single value. To maximize the variability captured by the P3 beta value, we calculated the sum across all P3-related beta weights (0–1.5 s) for each dual-task trial (Fig. 4E). The resulting P3 beta value was taken as a trial-by-trial measure of the degree of activation of the T1-P3 and T2-P3 components. Next, for each subject and ROI, we calculated the linear regression of the single-trial P3 beta weights on the single-trial parameter estimates (BOLD signal). To test for the significance of the resulting linear regression coefficients, we performed a non-parametric bootstrapping procedure to estimate 99% confidence intervals (5000 bootstrap samples, bias corrected and accelerated percentile method). Note that the possibility of false positives due to non-independent selection of ROIs, also referred to as "double dipping" (Kriegeskorte et al., 2009), is unlikely in this case, since the correlation with trial-by-trial ERP fluctuations is a test orthogonal to the initial contrast used to define the regions.

Results

Behavioral results: PRP effect

In all conditions, response times were comparable for trials with T1 on the left or T1 on the right of fixation. Therefore, we collapsed trials across T1 laterality for all subsequent analyses of behavioral data. Overall, response accuracy rates were high and only slightly, but significantly lower in dual-task trials ($94.7\% \pm 1.0$) than in single-task trials ($96.3\% \pm 0.7$; $t_{11} = 2.79$, $p = .018$; two-sided paired *t*-test). In dual-task trials, accuracies for the first response ($97.7\% \pm 0.5$) were higher than for the second response ($95.8\% \pm 0.7$; $F_{1,11} = 32.94$, $p < .001$), but response accuracies were not modulated by SOA ($F_{2,22} < 1$). Error trials were removed from all further analysis (behavioral, EEG, fMRI).

The mean RT in single-task trials was 534 ± 24 ms. In accordance with the classical PRP model (Pashler, 1994; Pashler and Johnston, 1989), RT2 increased significantly with a decreasing SOA (Fig. 3A). RT1 showed a much smaller, yet consistent and significant increase with a decreasing SOA. RT2 increased by 350 ms as SOA decreased from 800 to 100 ms, yielding an overall slope of -0.5 , while RT1 increased by 70 ms over the same range, resulting in a slope of -0.1 . Taking only the 100 and 300 ms SOAs into account, the slopes are -0.21 for RT1 and -0.91 for RT2, which is close to the theoretical slope of -1 predicted by the classical PRP model for short SOAs. The *F* ratios underline the difference in magnitude between the main effects of SOA for RT1 and RT2 (RT1: $F_{2,22} = 12.34$, $p < .001$; RT2: $F_{2,22} = 197.35$, $p < .001$). For RT1, post-hoc tests revealed significant differences between SOA 100 and 300 ($t_{11} = 4.75$, $p < .001$), SOA 100 and 800 ($t_{11} = 4.07$, $p < .002$), but not between SOA 300 and 800 ($t_{11} = 1.87$, $p = .088$). For RT2, post-hoc tests revealed significant differences between SOA 100 and 300 ($t_{11} = 16.26$, $p < .001$), SOA 100 and 800 ($t_{11} = 16.00$, $p < .001$), and between SOA 300 and 800 ($t_{11} = 9.28$, $p < .001$; two-sided paired *t*-tests).

Next, we analyzed RT1-RT2 correlations across SOAs. If central T2 processing is indeed postponed by central processing of T1, then RT1 and RT2 should be more strongly correlated at shorter SOAs. As can be seen in Fig. 3B, the average Pearson correlation coefficient significantly dropped from .76 at SOA 100 and .65 at SOA 300 to .20 at SOA 800 ($t_{11} = 8.36$, $p < .001$, and $t_{11} = 7.69$, $p < .001$, two-sided paired

Table 1

Resulting SPM clusters and peaks for contrasts “dual-task>single-task”, and “SOA100>SOA800”, thresholded at $p < .001$ (uncorrected). Cluster size in voxels ($3 \times 3 \times 3$ mm); peak t value (11 degrees of freedom); x, y, z coordinates in MNI space; brain region; approximate Brodmann’s area (BA); cortical peak index (#). Brain regions in bold font indicate regions with significant trial-by-trial covariation with the P3 component.

Contrast	Size	t	x	y	z	Brain region	BA	#
<i>Dual-task>single-task (mean of single tasks)</i>								
5005	10.97	−54	6	45		L precentral gyrus	6/44	1
	10.09	18	−6	60		R superior frontal gyrus	6	2
	10.08	42	−36	45		R inferior parietal lobule	2/40	3
	10.04	30	0	54		R middle frontal gyrus		4
	9.81	−21	−3	54		L superior frontal gyrus	6	5
	9.14	−30	−27	63		L precentral gyrus	4/6	6
	8.86	−15	0	75		L superior frontal gyrus	6	7
	8.37	−39	−39	45		L inferior parietal lobule	2	8
	8.16	33	−45	60		R superior parietal lobule		9
	7.91	36	−18	54		R precentral gyrus	6	10
555	7.14	9	−15	−6		R thalamus		
	6.91	−12	−18	−3		L thalamus		
192	6.41	57	9	39		R precentral gyrus	6/44	11
	6.01	39	3	30		R precentral gyrus	44	12
175	6.00	6	−54	−9		R cerebellum		
	4.98	−12	−48	−15		L cerebellum		
95	5.62	45	−60	0		R middle temporal gyrus		
<i>Dual-task>single-task (sum of single tasks)</i>								
60	5.75	−24	3	48		L middle frontal gyrus		13
	4.41	−27	3	66		L superior frontal gyrus		14
42	4.81	18	−48	66		R superior parietal lobule		15
	4.34	33	−48	60		R superior parietal lobule		16
<i>SOA100>SOA800</i>								
175	7.32	−45	30	9		L inferior frontal gyrus	45	17
	6.06	−42	21	6		L inferior frontal gyrus	44/45	18
136	5.45	3	27	15		R anterior cingulate cortex	24/32	19
	4.84	12	39	18		R anterior cingulate cortex	24/32	20
	4.79	−6	42	15		L anterior cingulate cortex	24/32	21
	4.76	−3	39	12		L anterior cingulate cortex	24/32	22

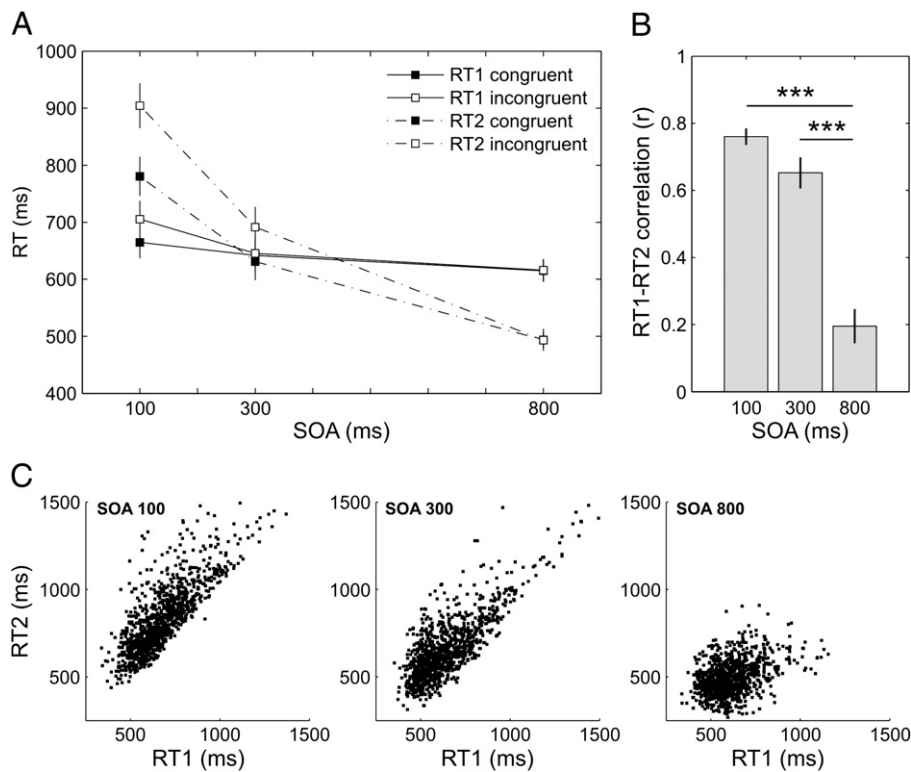


Fig. 3. Behavioral results in the dual-task conditions. (A) Average reaction times (RTs) at SOAs 100, 300, and 800 ms for responses to the first target (RT1, solid lines) and to the second target (RT2, dashed lines), separately for congruent and incongruent trials (filled and open squares, respectively). Error bars represent standard error of the mean (\pm SEM). (B) Average Pearson correlations (r) between RT1 and RT2 for all SOAs. Error bars represent standard error of the mean (\pm SEM). (C) Scatter plot of single-trial RT1 and RT2 data from all subjects to illustrate RT1–RT2 correlations across SOAs.

t-tests). The correlation coefficients at the short SOAs were not significantly different from each other ($t_{11} = 1.99$, $p = .07$; Fisher z-transformed coefficients). The strong influence of RT1 fluctuations on the postponement of task 2 at short SOA is in accordance with Pashler's notion of a central bottleneck, where the slowing in the first task is propagated onto the second task (Pashler, 1994). For an illustration of the significant increase in RT1–RT2 correlation at short SOAs, Fig. 3C plots single trial RTs across all subjects.

Behavioral results: crosstalk effects

Comparison between congruent and incongruent trials allows for the analysis of crosstalk between T1 and T2 processing. Crosstalk is defined as an effect of the congruency of the two target responses (here, both larger or both smaller than 5) on RT1 and RT2, respectively (Logan and Schulkind, 2000). Our data show that crosstalk from T1 to T2 in the RT2 data was significantly larger than backward crosstalk from T2 to T1 in the RT1 data ($61.4 \text{ ms} \pm 5.7$ versus $15.0 \text{ ms} \pm 3.9$; $t_{11} = 9.52$, $p < .001$). In both cases, crosstalk was significant (RT1: $F_{1,11} = 15.13$, $p < .003$; RT2: $F_{1,11} = 115.22$, $p < .001$). As indicated by the significant “SOA \times congruency” interaction (RT1: $F_{2,22} = 7.22$, $p < .01$; RT2: $F_{2,22} = 42.34$, $p < .001$), crosstalk was more pronounced at short SOAs: for RT1, significant backward crosstalk was found only at SOA 100 ($40.5 \text{ ms} \pm 8.6$; $t_{11} = 4.69$, $p < .001$), but not at SOA 300 ($3.4 \text{ ms} \pm 8.6$; $t_{11} = 0.40$) and SOA 800 ($1.2 \text{ ms} \pm 5.5$; $t_{11} = 0.22$); for RT2, crosstalk was significant at SOA 100 ($124.1 \text{ ms} \pm 11.1$; $t_{11} = 11.22$, $p < .001$) and SOA 300 ($60.7 \text{ ms} \pm 9.4$; $t_{11} = 6.43$, $p < .001$), but not at SOA 800 ($-0.7 \text{ ms} \pm 8.4$; $t_{11} = -0.08$).

EEG results: single-task

We started with a simple analysis of ERPs in single-task trials, aiming only to verify the capacity of the multiple regression procedure to separate events unfolding over time. Fig. 4B shows the results of the multiple linear regression procedure with three spatio-temporal profiles (T1–N1 ipsi-lateral, T1–N1 contra-lateral, T1–P3) applied to single-target trials. The betas for the contra-lateral N1 (T1–N1 contra, collapsing T1L–N1 for left targets and T1R–N1 for right targets) show a clear peak at approx. 200 ms. As expected, the betas for the ipsi-lateral N1 (T1–N1 ipsi, collapsing T1L–N1 for right targets and T1R–N1 for left targets) do not exhibit any clear-cut peak. The P3 betas (T1–P3, collapsed for left and right target trials) peak at 496 ms, therefore approximately 100 ms later than the first P3-related GFP peak at 400 ms, but well at the center of the broader P3-related GFP maximum ranging from 400 to ~600 ms (Fig. 4A). For each time point (1.5 s at 250 Hz = 375 points), we performed a bootstrapping procedure to estimate the confidence interval (5000 bootstrap samples, bias corrected and accelerated percentile method, alpha level = 0.05/375). In Figs. 4B–F, time points whose confidence interval did not contain zero are marked with a gray horizontal bar to indicate significance; if significant time points fall within a consecutive series of at least 10 significant points (40 ms), they are color-coded according to the condition to indicate significant components. Fig. 4B shows that we found significant time points between 152 and 212 ms for the contra-lateral T1–N1, and between 272 and 732 ms for the T1–P3. Importantly, the average correlation between contra-lateral T1–N1 and T1–P3 beta time-courses was not significantly different from zero (average Pearson's $r = -.11$, $t_{11} = 1.61$, $p = .13$, two-sided t -test; Fisher z-transformed coefficients), proving that the components could be reliably separated in single-task trials.

EEG results: dual-task

In a second step, the multiple regression procedure was used to parse the event-related activity in dual-task trials. As can be seen in

Fig. 4C, the T1–N1 peaking at approx. 200 ms was reliably recovered for all SOAs; bootstrapping revealed significant time points at the corresponding T1–N1 peak time (SOA 100: 160–228 ms; SOA 300: 168–216 ms; SOA 800: 180–216 ms). For SOAs 300 and 800, later significant time ranges at approx. 1000 ms were likely caused by residual noise in the frequency range of the N1. Fig. 4D shows that the T2–N1 could reliably be recovered for SOAs 100 and 800, at time ranges in accordance with stimulus-locking of the N1 (SOA 100: 272–308 ms; SOA 800: 968–1012 ms). For SOA 300, however, the peak within the expected T2–N1 time range at approx. 500 ms failed to reach significance. This reduction of the T2–N1 at SOA 300 might have been caused by residual noise in the EEG data, or alternatively, could be related to the fact that at SOA 300 the T1–P3 was maximally expressed, and therefore reduced the magnitude of the sensory potential evoked by a simultaneous distracting event, as has previously been reported (Rockstroh et al., 1992; Sigman and Dehaene, 2008).

The results of the multiple linear regression procedure for P3 activity in dual-task trials is shown in Figs. 4E–F. The T1–P3 could be recovered at all SOAs (Fig. 4E), with peaks within the expected time range of approx. 500 ms after T1 onset (SOA 100: 292–912 ms; SOA 300: 316–956 ms; SOA 800: 296–700 ms). Since we used a single T1–P3 template for targets presented on the left and on the right of fixation, the beta weights shown in Fig. 4E represent the overlap of T1–P3 and T2–P3 related activity in dual-task trials. As a consequence, at SOAs 100 and 300, this overlap leads to a superposition of the components; as can be seen, the beta weights in these conditions exhibit a slower decrease after the inflection point than in the single-task condition. At SOA 800, however, the T2–P3 is clearly separable from the T1–P3, peaking between 1168 and 1324 ms. To separate T2–P3 from T1–P3 related activity, we applied a subtraction procedure which has been used in a large number of previous ERP studies (Luck et al., 2000); this method assumes a linear superposition of EEG signals. Here, we subtracted the grand-average single-task beta weights (Fig. 4B) from the individual dual-task beta weights. The resulting T2–P3 “difference waves” in Fig. 4F clearly show that the T2–P3 was reliably recovered for all SOAs (SOA 100: 796–968 ms; SOA 300: 792–988 ms; SOA 800: 1160–1324 ms). In contrast to the T2–N1 component, the T2–P3 did not remain time-locked to the stimulus at SOAs 100 and 300, where latencies of 600 and 800 ms, respectively, would have been expected under stimulus-locking. At SOA 800, however, the observed peak falls within the expected time range (1300 ms). Thus, within the behavioral PRP interference regime at short T1–T2 SOAs, the T2–P3 peaks were shifted towards longer latencies. Note that for SOA 800, the earlier peak around 900 ms did not reach significance, but has been reported previously and might indicate an anticipation or preparation of the second task (Sigman and Dehaene, 2008).

To test for the significance of the observed T2–P3 latency shifts, we estimated the individual T2–P3 peak latencies by determining the beta weight maxima between T2 onset and 1500 ms after T1 onset, and compared them to the expected stimulus-locked latencies. For SOA 100, the T2–P3 latency was estimated at 776 ± 45 ms, therefore significantly delayed by 280 ms, given its 496 ms latency in single-target trials ($t_{11} = 5.9$, $p < .001$). For SOA 300, the average T2–P3 peak was estimated at 670 ± 46 ms, thus yielding a delay of 174 ms which was also significant ($t_{11} = 3.67$, $p < .005$). For SOA 800, the estimated latency of 504 ± 22 ms almost perfectly coincided with the stimulus-locked latency of 496 ms, based on the single-task analysis ($t_{11} < 1$). Importantly, T2–P3 latency shifts at short SOAs were of comparable magnitude as the behavioral effects in the group (latency shifts: 280 ms at SOA 100, 174 ms at SOA 300; as compared to the RT2 effects [RT2 minus single-task RT]: 299 ms at SOA 100, 127 ms at SOA 300). Overall, there was good correspondence between the T2–P3 latency shifts observed using the spatio-temporal template method and “raw” grand average ERPs from parietal electrodes (Supplementary Fig. S2).

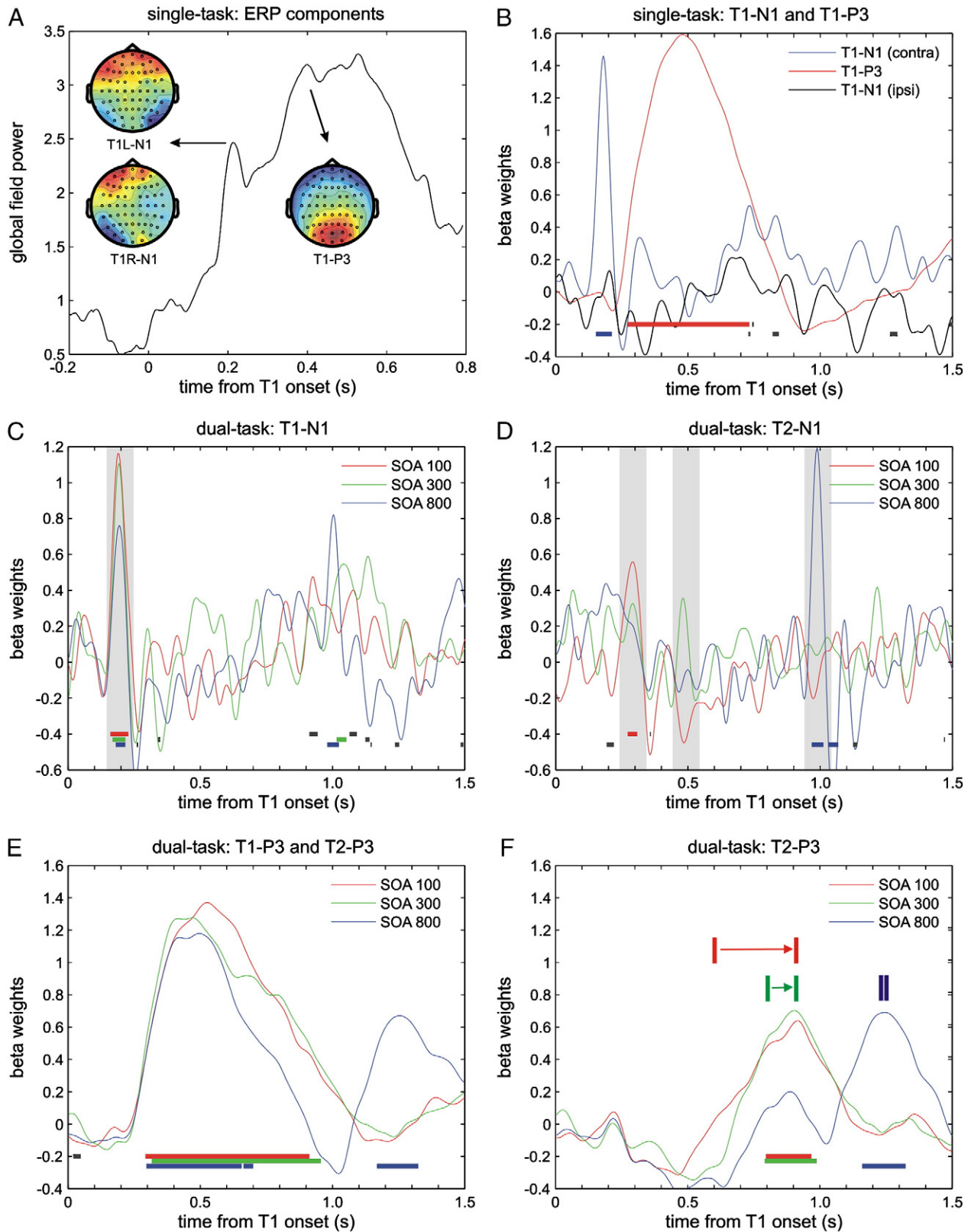


Fig. 4. Event-related potential (ERP) analysis. (A) Global field power (GFP) of ERPs in single-task trials. The 2D scalp topographies (small circles represent electrodes) show the N1 topography evoked by left targets (T1L-N1), N1 topography evoked by right targets (T1R-N1), and P3 topography evoked by left and right targets (T1-P3). (B) Results of the multiple regression applied to single-task trials. Beta weights for T1-N1 (blue, black) and T1-P3 (red) are plotted against time from T1 onset. (C–F) Results of the multiple regression applied to dual-task trials. (C) T1-N1 beta weights are plotted for different SOAs. (D) T2-N1 beta weights. Transparent gray bars indicate time-windows for stimulus-locked N1. (E) Overlap of T1-P3 and T2-P3 beta weights in dual-task trials for different SOAs. (F) Results of the subtraction of single-task T1-P3 beta weights (shown in B) from T1-P3/ T2-P3 beta weights in dual-tasks (shown in E). Colored arrows and vertical bars illustrate the temporal delay of T2-P3 responses. In dual-task plots (C–F), red lines indicate SOA 100, green lines indicate SOA 300, blue lines indicate SOA 800. Gray horizontal bars (B–F) indicate significant time points (deviation from zero); significant time points within a consecutive series of at least 10 significant time points (40 ms) are color-coded according to condition.

Taken together, we were able to decompose dual-task ERPs into subcomponents and detect a shift in the T2-P3 latency, directly reflecting the response delay characteristic of the PRP phenomenon.

EEG results: extracted beta weights

The next step was to characterize trial-by-trial variability in ERPs. We extracted trial-by-trial beta weights for each subject and for each component in time windows centered on the peak latencies (T1-N1 and T2-N1: 200 ms post-target; T1-P3: 500 ms post-T1; T2-P3: SOA 100, 776 ms post-T2; SOA 300, 670 ms post-T2; SOA 800, 504 ms post-T2). Fig. 5A shows the grand average beta weights for all components as a function of SOA in dual-task trials. T1-related beta weights were significantly larger than T2-related beta weights for P3 ($t_{11} = 3.93$, $p < .01$, two-sided paired t -test), but not for N1 ($t_{11} = 1.77$, $p = .11$). The factor “SOA” did not significantly modulate the extracted beta weights, neither for N1 (T1-N1: $F_{2,22} = 3.35$, $p = .064$; T2-N1: $F_{2,22} = 3.42$, $p = .057$), nor for P3 (T1-P3: $F_{2,22} < 1$; T2-P3: $F_{2,22} < 1$), and also not for the sum of T1-P3/T2-P3 beta weights ($F_{2,22} < 1$; repeated measures ANOVA). Finally, since the single-trial beta weights were meant to be used in a multiple regression of the fMRI data, we checked their cross-correlation, separately for each SOA, and obtained three correlations matrices for each subject. Fig. 5B shows the resulting correlation matrices averaged across subjects. With the exception of the correlation between T1-P3 and T2-P3, which was significant for each SOA (SOA 100, $r = .57$; SOA 300, $r = .55$; SOA 800, $r = .58$; all $p < .001$; Fisher z -transformed coefficients), correlations between ERP components were low (between $-.12$ and $.05$) and not significant.

fMRI results: statistical parametric maps

We next examined fMRI evidence for single- and dual-task effects. Both single-task (“single-task>baseline”) and dual-task (“dual-

task>baseline”) contrast SPMs showed a wide range of significant clusters in the occipital early visual, parietal, motor, and prefrontal (superior and middle frontal gyrus) cortical areas, as well as in the thalamus and cerebellum. As can be seen in Fig. 6A, the contrast “dual-task>mean of single-tasks”, reflecting the additional demands of the entire second task plus dual-task costs (Marois and Ivanoff, 2005), revealed significant clusters primarily in the parietal (including left and right inferior parietal lobe, and superior parietal lobe) and frontal areas (including left and right precentral gyrus, right middle frontal gyrus, and right superior frontal gyrus; see Table 1 for all significant clusters and cluster peaks). A cluster in the right middle temporal gyrus, most probably located in motion-sensitive area MT (Tootell et al., 1995), also showed an increased activation in the dual-task condition as compared to the single-task condition. Activation of area MT is most likely due to the effect of apparent motion (“phi phenomenon”), evoked by the target numbers successively flashing left and right (or, vice versa) of fixation; apparent motion related activity in MT has been reported for a similar paradigm (Goebel et al., 1998). Fig. 6B shows that the contrast “dual-task>sum of single-tasks”, which has been proposed to be a suitable yet conservative test for dual-task specific effects (Szameitat et al., 2011), revealed significant activation in the left middle and superior frontal gyrus, as well as in the right superior parietal lobule. The contrast “SOA 100>SOA 800”, which has previously been used (“short SOA>long SOA”) in a number of studies on dual-task processing (Herath et al., 2001; Jiang, 2004; Jiang et al., 2004), revealed two significant clusters, one in the left inferior frontal gyrus (IFG), and the other in the rostral part of the ACC (Fig. 6C). All inverse contrasts yielded no significant clusters.

fMRI correlates of trial-by-trial ERP variability

Finally, we cross-correlated the single-trial ERP variability with the simultaneously recorded fMRI signals, in order to obtain a more

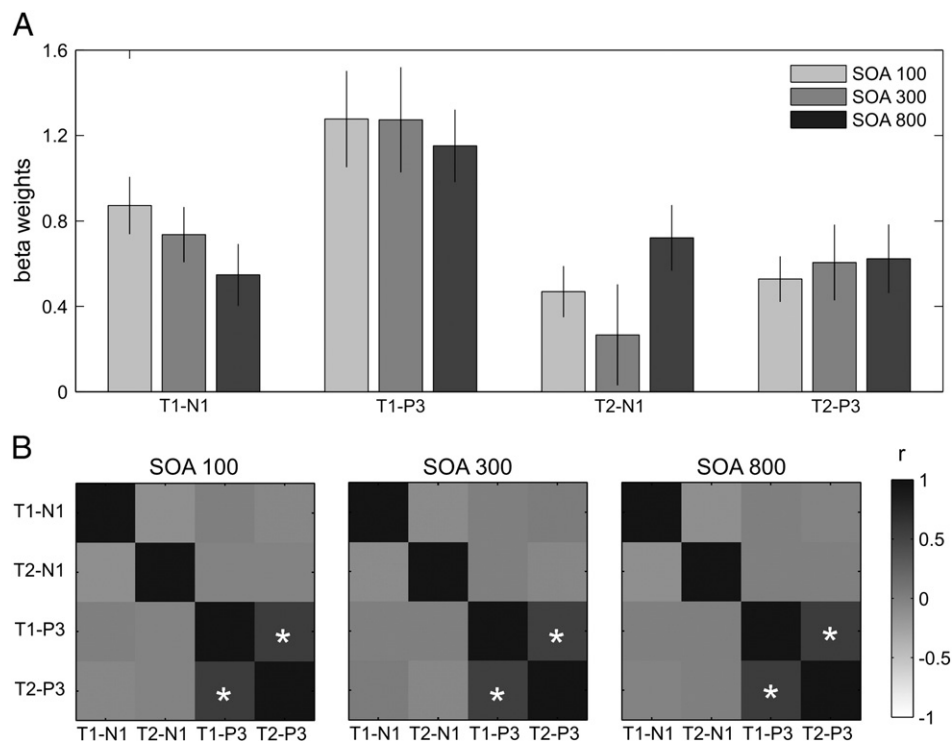


Fig. 5. Extracted N1 and P3 peak beta weights. (A) Average extracted beta weights for dual-task ERP components (T1-N1, T1-P3, T2-N1, T2-P3) at all SOAs (100, 300, 800). Error bars represent standard error of the mean (\pm SEM). (B) Average cross-correlation matrices for extracted beta weights at all SOAs. Asterisks indicate significant ($p < .05$) Pearson coefficients (r).

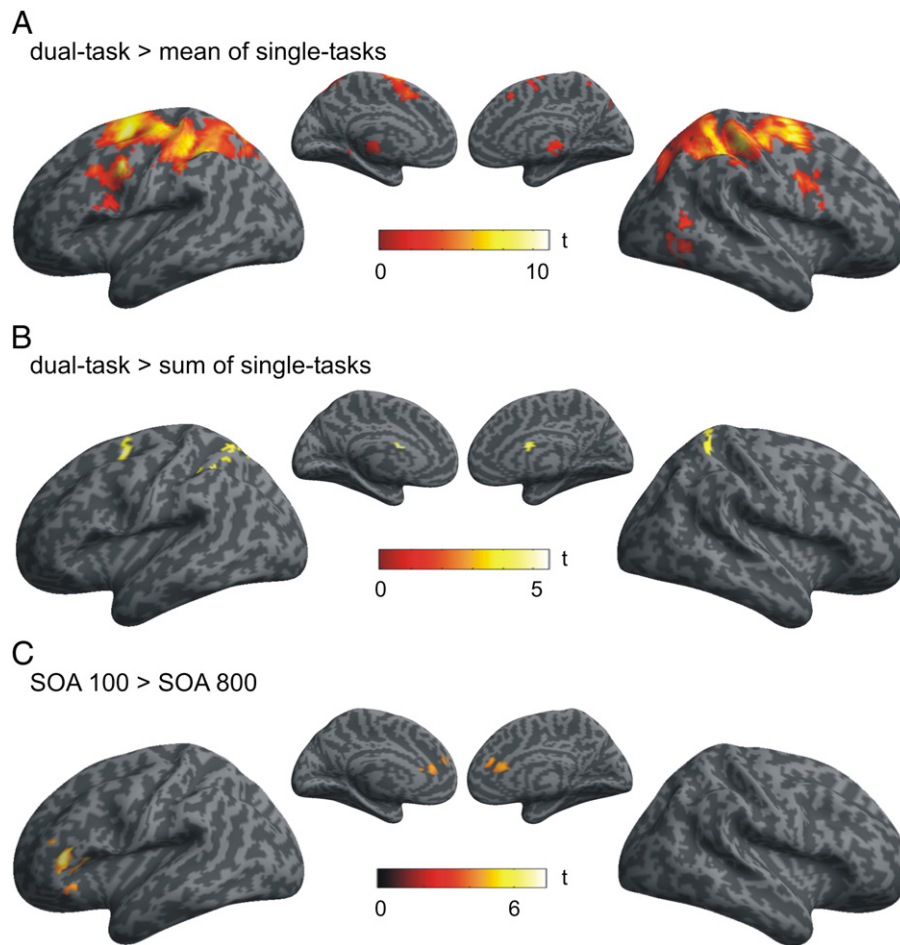


Fig. 6. Statistical parametric maps (random effects). A) The contrast “dual-task>mean of single-tasks” yielded a number of significant clusters in parietal, frontal and prefrontal cortical areas, as well as in the right area hMT+. B) The contrast “dual-task>sum of single-tasks” revealed significant clusters in the left middle/frontal gyrus and the right superior parietal lobule. C) The contrast “SOA 100>SOA 800” revealed only two significant clusters, in the rostral ACC, and in the left inferior frontal gyrus. Threshold height $p < .05$ corrected at the cluster level using an auxiliary (uncorrected) voxel threshold of $p < .001$. Statistical parametric maps are superimposed onto the lateral and medial aspects of an inflated cortical surface of a canonical average brain. Color bars show t values ($df = 11$).

selective neural correlate of the “central stage” associated with the P3 component and responsible for the behavioral PRP effect (see methods). The EEG-informed *whole-brain* fMRI analysis did not yield any significant clusters, even at more lenient thresholds ($p < .01$), neither for the contrast “T1-P3 parametric modulator>baseline”, which aimed at identifying brain regions whose BOLD signals correlated with the peak T1-P3 amplitudes in dual-task trials, nor for the contrast “T2-P3 parametric modulator>baseline”. The second EEG-informed fMRI analysis was restricted to cortical ROIs based on both “dual-task>single-task” contrasts and the “SOA 100>SOA 800” contrast (Table 1, excluding area MT), and aimed at identifying regions whose BOLD signals covaried with the beta weights of the overlapping T1-P3 and T2-P3 components in dual-task trials. To that aim, we calculated the linear regression of the single-trial P3 beta weights on the single-trial parameter estimates (BOLD signal), separately for each subject and ROI. This ROI based fMRI analysis yielded significant negative linear regression coefficients in two sets of homotopic regions in the left and right inferior parietal lobe (peak #8: CI = [−0.173, −0.003]; peak #3: CI = [−0.313, −0.028]), and in the left and right precentral gyrus (peak #1: CI = [−0.331, −0.039]; peak #11: CI = [−0.166, −0.002]; 99% confidence intervals based on non-parametric bootstrapping). Using parametric two-sided t -tests to test for the significance of linear regression coefficients yielded similar significant results (peak #8: $t_{11} = -2.45$, $p = .032$; peak #3: $t_{11} = -2.44$, $p = .033$; peak #1: $t_{11} = -2.46$, $p = .032$; peak #11: $t_{11} = -2.04$, $p = .066$).

fMRI correlates of inter-individual variability in PRP magnitude

We also searched for BOLD activity that covaried with a neurophysiological marker of the magnitude of the PRP effect across subjects (Herath et al., 2001; Jiang et al., 2004). To this aim, we correlated BOLD activity levels in the selected cortical ROIs with the observed T2-P3 latency shifts at SOA 100 across subjects. Dell’Acqua et al. (2005) have reported a significant linear relationship between the slowing of the T2-P3 and the PRP effect, suggesting an overlap between central dual-task interference and the mechanisms responsible for the generation of P3 activity. In our study, individual T2-P3 latency delays were determined as described in the EEG sections. Individual BOLD activity levels were obtained by subtracting SOA 800 from SOA 100 beta values of the first-level GLM for each subject. A single area in the left IFG showed a significant positive correlation between T2-P3 slowing and BOLD activity (peak #18: Pearson’s $r = .61$, $p = .034$). A positive relation indicates that, as expected, a larger T2 delay is associated with a higher BOLD, presumably to a greater duration of activation in a key area thought to be involved in the central bottleneck (Dux et al., 2006, 2009).

Discussion

In this study, our aim was to probe the brain mechanisms underlying the PRP effect in dual-task processing by simultaneously recording EEG and fMRI responses. As expected, our behavioral data

showed a lengthening of RT2 and significant RT1–RT2 correlations at short SOAs, which are considered as the hallmarks of the PRP (Pashler, 1994; Pashler and Johnston, 1989). Furthermore, we identified ERP alone, fMRI alone, and joint ERP–fMRI correlates of the PRP effect, which significantly constrain the theoretical interpretation of this phenomenon. Finally, we also observed crosstalk between the T1 and T2 decisions. Each of these points is discussed in turn.

ERP decomposition of the PRP effect

In accordance with earlier ERP studies of the PRP effect, we found the N1 component to be stimulus-locked for both targets T1 and T2 at all SOAs (Brisson and Jolicoeur, 2007; Sigman and Dehaene, 2008). Furthermore, we observed no suppression of the N1 component evoked by the second target (T2–N1) during the PRP. Together, these data provide evidence for a *post-perceptual* bottleneck in our experimental paradigm (Vogel et al., 1998). Similarly, both amplitude and latency of the P3 component evoked by the first target (T1–P3) remained unaffected by the SOA. The latency of the T2–P3, however, showed a substantial delay at short SOAs, while T2–P3 amplitude was not modulated. In contrast to previous studies (Arnell et al., 2004; Luck, 1998), our results showed T2–P3 latency shifts of comparable magnitude as the behavioral effects on RT2. Similar postponements of T2 processing have been reported for a P3 component evoked by auditory and visual stimuli (Sigman and Dehaene, 2008), as well as for the lateralised readiness potential in dual-tasks (Jentzsch et al., 2007). One ERP study reported a significant correlation between T2–P3 latency delays and RT2 postponement across participants (Dell'Acqua et al., 2005). However, there are two main differences between our study and the findings reported by Dell'Acqua. First, Dell'Acqua and colleagues based their analysis on a P3-like component with a rather frontal topography, similar to a novelty-P3 (Friedman et al., 2001), while we analyzed a P3 (P3b) component with parietal focus (Donchin and Coles, 1988; Verleger et al., 2005). Second, their study found a significant correlation between T2–P3 latency and RT2 for a subset of subjects (N = 12) who showed large P3 amplitudes; due to our smaller sample size we could not perform a comparable analysis based on a median split. Thus, a conclusion on this point will have to await further research.

Our ERP results are in good agreement with findings in related attentional blink and masking experiments suggesting a decomposition of processing into perceptual ERPs up to ~270 ms after target onset, followed by a P3 reflecting access to a central stage of distributed processing (Del Cul et al., 2007; Sergent et al., 2005). Furthermore, our finding of a rigid delay of the T2–P3 without a change in amplitude is compatible with the classical model of a serial bottleneck postponing processing of the second task (Pashler, 1994).

fMRI correlates of the PRP

The whole-brain fMRI analysis using the contrast “dual-task > mean of single-tasks” yielded a bilateral network of parietal and frontal regions, as well as clusters in the thalamus and cerebellum. A fronto-parietal network of regions has been linked to dual-task processing limits (and further capacity limits in information processing) in a number of previous studies (Marois and Ivanoff, 2005). The contrast “dual-task > sum of single-tasks”, which has been proposed to be a particularly suitable yet conservative test for dual-task specific effects (Szameitat et al., 2011), revealed significant activation in the left middle and superior frontal gyrus, as well as in the right superior parietal lobule. The contrast “SOA 100 > SOA 800”, which has previously been used (“short SOA > long SOA”) with different outcomes (Herath et al., 2001; Jiang, 2004; Jiang et al., 2004), resulted in only two prefrontal cortical regions, one in rostral ACC and the other in the left IFG. The ACC is generally known to be

involved in cognitive control in a variety of tasks (Bush et al., 2000); more specifically, the rostral ACC has been shown to be activated when conflicts between stimulus–response associations need to be resolved when performing two tasks simultaneously, as compared to performing them in succession (Dreher and Grafman, 2003). In our paradigm, the SOA 100 condition resembles a simultaneous situation, since the second target appears before the response to the first target has been executed; in the SOA 800 condition, however, the second target appears only after the response to the first target. Activity in the lateral prefrontal cortex associated with dual-task processing has been reported previously, and a major role of the inferior frontal sulcus (IFS) has been proposed (Schubert, 2008; Schubert and Szameitat, 2003; Szameitat et al., 2006). Related studies have linked the left IFS to the management of interfering response alternatives, e.g., in task switching paradigms (Dove et al., 2000). Recently, two studies provided evidence for the involvement of the left posterior lateral prefrontal cortex in dual-task limitations, using time-resolved fMRI (Dux et al., 2006) and the extensive training of a multitasking situation (Dux et al., 2009). Both studies located the area strongly involved in dual-task processing in the inferior frontal junction (Brodmann area 9). Compared to the abovementioned studies, the region we observed to be involved in dual-task processing is located slightly more anterior and more ventral, in the left IFG. Interestingly, an exploratory analysis of our EEG–fMRI data revealed that BOLD activity in the left IFG showed a significant positive inter-subject correlation with T2–P3 latency, suggesting that central processes regulating the attentional demands between both tasks are more active for subjects with larger T2–P3 postponement. Taken together, our finding of the involvement of the ACC and left IFG in dual-task processing appears to speak against a passive queuing account of the PRP (Jiang et al., 2004; Pashler, 1994). Indeed, the central bottleneck model predicts purely delayed activation, but not in the presence of additional activity at short lags. fMRI activity delays corresponding to the PRP have been observed at distributed sites, particularly in the inferior parietal and prefrontal cortex, in a recent study with heightened temporal resolution (Sigman and Dehaene, 2008). Nevertheless, the presence of increased activity at short lags, over and above pure delays, supports models additionally involving an active monitoring component (Logan and Gordon, 2001; Sigman and Dehaene, 2006).

fMRI–EEG correlations

In our ROI based EEG-informed fMRI approach we restricted the statistical analysis to the cortical regions identified by both “dual-task > single-task” contrasts and the “SOA 100 > SOA 800” contrast. This analysis revealed that BOLD activity in two bilateral regions in the inferior parietal lobe and precentral gyrus covaried with P3 related activity on a trial-by-trial basis. The plausibility of these effects, which were significant at uncorrected 99% confidence levels, is increased by the observation of significant results in bilateral *homotopic* regions. Similar cortical regions have recently been shown to be related to the PRP in a time-resolved fMRI study, together with bilateral dorsolateral prefrontal cortex (Sigman and Dehaene, 2008). Surprisingly, the correlation between trial-by-trial variations in P3 size and fMRI activity was negative in all three regions. At first sight, this finding seems to contradict expectations of a stronger fMRI activation accompanying the more intense brain activity directly reflected in P3 size. The negative correlation may however be explained by considering that fMRI accumulates over time, while in ERPs we only measured the amplitude of the P3. Within the framework of accumulation-of-evidence models, a higher and sharper P3 peak indicates faster decision making (i.e., a steeper slope of the accumulation-of-evidence process), and may therefore result in a reduced total fMRI activation in the relevant decision-making circuit. For instance, in a similar analysis of trial-by-trial ERP variability,

Sergent et al. (2005) observed a larger and earlier T1-evoked P3 peak on trials that did *not* lead to an attentional blink on a subsequent T2 target, which was interpreted as indicating that the decision bottleneck was occupied for a shorter, more compact period on these trials. From these results, the expectation would be that a sharper P3 should correlate with a less intense overall fMRI signal, and this is exactly what we observed in the present simultaneous EEG–fMRI recordings.

Taken together, our findings based on the EEG-informed fMRI analysis strengthen the conclusion that bilateral areas in the inferior parietal lobe and precentral gyrus participate in a distributed “global neuronal workspace” system that underlies the generation of the P3 component and may be one of the key cerebral underpinnings of the PRP bottleneck (Dehaene and Naccache, 2001; Del Cul et al., 2007; Sergent et al., 2005). To elucidate the potential relationship between serial information processing during the PRP and the global workspace, further EEG-combined fMRI studies of the PRP, in particular studies simultaneously probing the PRP effect and the closely related attentional blink (AB) phenomenon (Arnell and Duncan, 2002; Jolicoeur, 1999; Wong, 2002), are needed.

Crosstalk effects

Previous PRP studies have reported backward crosstalk (i.e., a dependence of RT1 on the response that is required for the second stimulus) when highly similar tasks have to be performed [(Logan and Delheimer, 2001; Logan and Schulkind, 2000), but see (Miller, 2006)]. In agreement with this earlier work, the two identical number-comparison tasks used in our study resulted in significant crosstalk effects at SOA 100. Backward crosstalk seems difficult to reconcile with the strictly serial bottleneck model, since they suggest that T2 processing may start before T1 processing has been completed. Accordingly, the finding of backward crosstalk in PRP experiments has been interpreted as supporting central resource sharing models (Navon and Miller, 2002; Tombu and Jolicoeur, 2003) whereby the two tasks are performed partially in parallel and with continuous variable relative priorities. As a post-hoc analysis, we attempted to separate the bottleneck and resource sharing interpretations by looking for a critical differential prediction concerning inter-individual variability. The resource sharing model predicts that participants with more backward crosstalk of T2 on T1 should have a smaller PRP effect; the argument builds on the assumption that crosstalk in RT1 indicates that T2 processing has already been started in parallel to T1 processing, and therefore should be completed earlier, i.e., a smaller PRP effect. Thus, a negative relation between crosstalk and the PRP effect is predicted. Conversely, the bottleneck model predicts a positive relation, because more crosstalk means less efficient task processing and therefore slower RT2, precisely at short SOAs. We determined for each subject the size of the PRP effect following Jiang et al. (2004): $[\text{SOA } 100 (\text{RT}_1 + \text{RT}_2) - \text{SOA } 800 (\text{RT}_1 + \text{RT}_2)] / [\text{SOA } 800 (\text{RT}_1 + \text{RT}_2)]$. Using this definition, we found a significant *positive* correlation between backward crosstalk measured at SOA 100 and the PRP effect (Pearson's $r = .72$, $p = .008$), providing evidence in favor of the classical bottleneck model. How, then, can one explain the crosstalk effect in a serial bottleneck model? One possibility is insufficient stimulus selection (i.e., imperfect “filtering-out” of the irrelevant target). The present task involved the near-simultaneous presentation of two targets left and right of fixation, implying that spatial attention is required to select the relevant target and inhibit the other. Crosstalk may then be explained by a partial “leakage” of sensory evidence from the irrelevant target, resulting in T2-based sensory evidence contaminating the T1 decision. This possibility is made more likely by the finding that unattended and even subliminal digits can automatically access a representation of their magnitude (Dehaene et al., 1998; Naccache and Dehaene, 2001; Sackur et al., 2008). It builds upon the notion that the serial processing bottleneck

can be characterized as the accumulation of evidence towards a decision boundary (Sigman and Dehaene, 2005), and that it is likely that at short SOAs, both T1 and T2 contribute evidence towards either decision. For a further alternative how a bottleneck model can account for the occurrence of crosstalk see the study by Schubert et al. (2008) who used a PRP paradigm with additional subliminal response priming to vary pre-activation of the second task. Instead of a unique and discrete response-selection mechanism, Schubert et al. propose different response-selection subprocesses with response activation proceeding in parallel between tasks.

Concluding remarks

Although we observed significant correlations between trial-by-trial ERP variations and simultaneously recorded fMRI signals in predefined regions of interest, the fact that we did not find any significant regions by a *whole-brain* EEG-informed analysis, as for example in studies of the error-related negativity (Debener et al., 2005) or the go/nogo paradigm (Karch et al., 2010), is disappointing. The reasons could be twofold. First, there could have been a lack of meaningful variability in the analyzed ERP components. In both abovementioned studies the variability was primarily *across* experimental conditions, e.g., across low and high error rate trials in compatible and incompatible conditions, respectively. In our study, variability of ERP components was primarily *within* experimental conditions, since the factor “SOA” did not show any significant effect on the extracted components. Such *intrinsic* variability could be caused by random neuronal fluctuations which have previously been shown to significantly impact on perception (Hesselmann et al., 2008a,b; Monto et al., 2008), but their timescale might have been too slow for our fast event-related experimental design. Second, there could have simply been too much residual noise in our EEG signals due to the combined EEG–fMRI recording. We are confident that further advances in combined EEG–fMRI techniques (Laufs et al., 2008), together with ongoing improvements of independent component analysis (ICA) methods for noise removal and IC classification, including the semi-automatic (Viola et al., 2009) and automatic (Mognon et al., 2011) identification of artifactual IC components, may allow future PRP studies to determine single-trial measures of both P3 amplitude and latency for EEG data recorded simultaneously with fMRI, as shown recently for a simple target detection task (Warbrick et al., 2009). Such follow-up EEG–fMRI studies could eventually link subjects' response times and neuroimaging data to detailed models of the neuronal activity underlying the PRP (Sigman and Dehaene, 2006; Zylberberg et al., 2010).

Acknowledgments

This experiment was supported by INSERM, CEA, and the Human Frontiers Science Program. It constitutes part of a general research program on functional neuroimaging of the human brain which was sponsored by the Atomic Energy Commission (Denis Le Bihan). GH was supported by a Minerva fellowship (Max Planck Society), and would like to thank Jérémie Mattout for his invaluable support during the early EEG/fMRI recordings at SHFJ in Orsay, and Floris de Lange for the illustration of the hands (Fig. 2). The authors thank Laurent Larière at CEA/Neurospin for technical assistance, and two anonymous reviewers for constructive comments and suggestions.

Appendix A. Supplementary data

Supplementary data to this article can be found online at doi:10.1016/j.neuroimage.2011.03.017.

References

- Allen, P.J., Josephs, O., Turner, R., 2000. A method for removing imaging artifact from continuous EEG recorded during functional MRI. *Neuroimage* 12, 230–239.
- Arnell, K.M., Duncan, J., 2002. Separate and shared sources of dual-task costs in stimulus identification and response selection. *Cogn. Psychol.* 44, 105–147.
- Arnell, K.M., Helion, A.M., Hurdelbrink, J.A., Pasioka, B., 2004. Dissociating sources of dual-task interference using human electrophysiology. *Psychon. Bull. Rev.* 11, 77–83.
- Becker, R., Ritter, P., Moosmann, M., Villringer, A., 2005. Visual evoked potentials recovered from fMRI scan periods. *Hum. Brain Mapp.* 26, 221–230.
- Bell, A.J., Sejnowski, T.J., 1995. An information maximisation approach to blind separation and blind deconvolution. *Neural Comput.* 7, 1129–1159.
- Brett, M., Anton, J.-L., Valabregue, R., Poline, J.-B., 2002. Region of interest analysis using an SPM toolbox. 8th International Conference on Functional Mapping of the Human Brain, Sendai, Japan.
- Brisson, B., Jolicoeur, P., 2007. Electrophysiological evidence of central interference in the control of visuospatial attention. *Psychon. Bull. Rev.* 14, 126–132.
- Bush, G., Luu, P., Posner, M.I., 2000. Cognitive and emotional influences in anterior cingulate cortex. *Trends Cogn. Sci.* 4, 215–222.
- Coles, M.G.H., Gratton, G., Bashore, T.R., Eriksen, C.W., Donchin, E., 1985. A psychophysiological investigation of the continuous flow model of human information processing. *J. Exp. Psychol. Hum. Percept. Perform.* 11, 529–553.
- De Jong, R., 1993. Multiple bottlenecks in overlapping task performance. *J. Exp. Psychol. Hum. Percept. Perform.* 19, 965–980.
- Debener, S., Ullsperger, M., Siegel, M., Engel, A.K., 2006. Single-trial EEG–fMRI reveals the dynamics of cognitive function. *Trends Cogn. Sci.* 10, 558–563.
- Debener, S., Ullsperger, M., Siegel, M., Fiehler, K., von Cramon, D.Y., Engel, A.K., 2005. Trial-by-trial coupling of concurrent electroencephalogram and functional magnetic resonance imaging identifies the dynamics of performance monitoring. *J. Neurosci.* 25, 11730–11737.
- Dehaene, S., Naccache, L., 2001. Towards a cognitive neuroscience of consciousness: basic evidence and a workspace framework. *Cognition* 79, 1–37.
- Dehaene, S., Naccache, L., Le Clec'h, G., Koehlin, E., Mueller, M., Dehaene-Lambertz, G., van de Moortele, P.F., Le Bihan, D., 1998. Imaging unconscious semantic priming. *Nature* 395, 597–600.
- Del Cul, A., Baillet, S., Dehaene, S., 2007. Brain dynamics underlying the nonlinear threshold for access to consciousness. *PLoS Biol.* 5, 1–16.
- Dell'Acqua, R., Jolicoeur, P., Vespignani, F., Toffanin, P., 2005. Central processing overlap modulates P3 latency. *Exp. Brain Res.* 165, 54–68.
- Delorme, A., Makeig, S., 2004. EEGLab: an open source toolbox for analysis of single-trial EEG dynamics. *J. Neurosci. Meth.* 134, 9–21.
- Donchin, E., Coles, M.G., 1988. Is the P300 component a manifestation of context updating? *Behav. Brain Sci.* 11, 357–374.
- Dove, A., Pollmann, S., Schubert, T., Wiggins, C.J., von Cramon, D.Y., 2000. Prefrontal cortex activation in task switching: an event-related fMRI study. *Cogn. Brain Res.* 9, 103–109.
- Dreher, J.-C., Grafman, J., 2003. Dissociating the roles of the rostral anterior cingulate and the lateral prefrontal cortices in performing two tasks simultaneously or successively. *Cereb. Cortex* 13, 329–339.
- Dux, P.E., Ivanoff, J., Asplund, C.L., Marois, R., 2006. Isolation of a central bottleneck of information processing with time-resolved fMRI. *Neuron* 52, 1109–1120.
- Dux, P.E., Tombu, M.N., Harrison, S., Rogers, B.P., Tong, F., Marois, R., 2009. Training improves multitasking performance by increasing the speed of information processing in human prefrontal cortex. *Neuron* 63, 127–138.
- Eickhoff, S.B., Stephan, K.E., Mohlberg, H., Grefkes, C., Fink, G.R., Amunts, K., Zilles, K., 2005. A new SPM toolbox for combining probabilistic cytoarchitectonic maps and functional imaging data. *Neuroimage* 25, 1325–1335.
- Felleman, D.J., Van Essen, D.C., 1991. Distributed hierarchical processing in the primate cerebral cortex. *Cereb. Cortex* 1, 1–47.
- Friedman, D., Cycowicz, Y.M., Gaeta, H., 2001. The novelty P3: an event-related brain potential (ERP) sign of the brain's evaluation of novelty. *Neurosci. Biobehav. Rev.* 25, 355–373.
- Friston, K.J., Ashburner, J.T., Kiebel, S., Nichols, T.E., Penny, W.D., 2007. *Statistical Parametric Mapping—The Analysis of Functional Brain Images*. Elsevier.
- Friston, K.J., Holmes, A., Worsley, K., Poline, J., Frith, C., Frackowiak, R.S., 1994. Statistical parametric maps in functional imaging: a general linear approach. *Hum. Brain Mapp.* 2, 189–210.
- Goebel, R., Khorrarn-Sefat, D., Muckli, L., Hacker, H., Singer, W., 1998. The constructive nature of vision: direct evidence from functional magnetic resonance imaging studies of apparent motion and motion imagery. *Eur. J. Neurosci.* 10, 1563–1573.
- Greenhouse, S.W., Geisser, S., 1959. On methods in the analysis of profile data. *Psychometrika* 24, 95–112.
- Herath, P., Klingberg, T., Young, J., Amunts, K., Roland, P., 2001. Neural correlates of dual task interference can be dissociated from those of divided attention: an fMRI study. *Cereb. Cortex* 11, 796–805.
- Herrmann, C.S., Debener, S., 2008. Simultaneous recording of EEG and BOLD responses: a historical perspective. *Int. J. Psychophysiol.* 67, 161–168.
- Hesselmann, G., Kell, C.A., Eger, E., Kleinschmidt, A., 2008a. Spontaneous local variations in ongoing neural activity bias perceptual decisions. *PNAS* 105, 10984–10989.
- Hesselmann, G., Kell, C.A., Kleinschmidt, A., 2008b. Ongoing activity fluctuations in hMT+ bias the perception of coherent visual motion. *J. Neurosci.* 28, 14481–14485.
- Iannetti, G.D., Niaz, R.K., Wise, R.G., Jezzard, P., Brooks, J.C.W., Zambrenu, L., Vennart, W., Matthews, P.M., Tracey, I., 2005. Simultaneous recording of laser-evoked brain potentials and continuous, high-field functional magnetic resonance imaging in humans. *Neuroimage* 28, 708–719.
- Jentsch, I., Leuthold, H., Ulrich, R., 2007. Decomposing sources of response slowing in the PRP paradigm. *J. Exp. Psychol. Hum. Percept. Perform.* 33, 610–626.
- Jiang, Y., 2004. Resolving dual-task interference: an fMRI study. *Neuroimage* 22, 748–754.
- Jiang, Y., Saxe, R., Kanwisher, N., 2004. Functional magnetic resonance imaging provides new constraints on theories of the psychological refractory period. *Psychol. Sci.* 15, 390–396.
- Jolicoeur, P., 1999. Concurrent response-selection demands modulate the attentional blink. *J. Exp. Psychol. Hum. Percept. Perform.* 25, 1097–1113.
- Karch, S., Feuerrecker, R., Leicht, G., Meindl, T., Hantsch, L., Kirsch, V., Ertl, M., Lutz, J., Pogarell, O., Mulert, C., 2010. Separating distinct aspects of the voluntary selection between response alternatives: N2- and P3-related BOLD responses. *Neuroimage* 51, 356–364.
- Kriegeskorte, N., Simmons, W.K., Bellgowan, P.S.F., Baker, C.I., 2009. Circular analysis in systems neuroscience: the dangers of double dipping. *Nat. Neurosci.* 12, 535–540.
- Laufs, H., Daunizeau, J., Carmichael, D.W., Kleinschmidt, A., 2008. Recent advantages in recording electrophysiological data simultaneously with magnetic resonance imaging. *Neuroimage* 40, 515–528.
- Lehmann, D., Skrandies, W., 1980. Reference-free identification of components of checkerboard-evoked multichannel potential fields. *Electroencephalogr. Clin. Neurophysiol.* 48, 609–621.
- Logan, G.D., Delheimer, J.A., 2001. Parallel memory retrieval in dual-task situations: II. Episodic Memory. *Journal of Experimental Psychology: Learning, Memory and Cognition* 27, 668–685.
- Logan, G.D., Gordon, R.D., 2001. Executive control of visual attention in dual-task situations. *Psychol. Rev.* 108, 393–434.
- Logan, G.D., Schulkind, M.D., 2000. Parallel memory retrieval in dual-task situations: I. Semantic memory. *J. Exp. Psychol. Hum. Percept. Perform.* 26, 1072–1090.
- Luck, S.J., 1998. Sources of dual-task interference: evidence from human electrophysiology. *Psychol. Sci.* 9, 223–227.
- Luck, S.J., Woodman, G.F., Vogel, E.K., 2000. Event-related potential studies of attention. *Trends Cogn. Sci.* 4, 432–440.
- Mandelkow, H., Halder, P., Boesiger, P., Brandeis, D., 2006. Synchronization facilitates removal of MRI artefacts from concurrent EEG recordings and increases usable bandwidth. *Neuroimage* 32, 1120–1126.
- Mantini, D., Corbetta, M., Perrucci, M.G., Romani, G.L., Del Gratta, C., 2009. Large-scale brain networks account for sustained and transient activity during target detection. *Neuroimage* 44, 265–274.
- Marois, R., Ivanoff, J., 2005. Capacity limits of information processing in the brain. *Trends Cogn. Sci.* 9, 296–305.
- Mars, R.B., Debener, S., Gladwin, T.E., Harrison, L.M., Haggard, P., Rothwell, J.C., Bestmann, S., 2008. Trial-by-trial fluctuations in the event-related electroencephalogram reflect dynamic changes in the degree of surprise. *J. Neurosci.* 28, 12539–12545.
- Meyer, D.E., Kieras, D.E., 1997a. A computational theory of executive cognitive processes and multiple-task performance: 2. Accounts of the psychological refractory-period phenomena. *Psychol. Rev.* 104, 749–791.
- Meyer, D.E., Kieras, D.E., 1997b. A computational theory of executive cognitive processes and multiple-task performance: Part I. Basic mechanisms. *Psychol. Rev.* 104, 3–65.
- Miller, J., 2006. Backward crosstalk effects in psychological refractory period paradigms: effects of second-task response types on first-task response latencies. *Psychol. Res.* 70, 484–493.
- Mognon, A., Jovicich, J., Bruzzone, L., Buiatti, M., 2011. ADJUST: an automatic EEG artifact detector based on the joint use of spatial and temporal features. *Psychophysiology* 48, 229–240.
- Monto, S., Palva, S., Voipio, J., Palva, J.M., 2008. Very slow EEG fluctuations predict the dynamics of stimulus detection and oscillation amplitudes in humans. *J. Neurosci.* 28, 8268–8272.
- Naccache, L., Dehaene, S., 2001. Unconscious semantic priming extends to novel unseen stimuli. *Cognition* 80, 215–229.
- Navon, D., Miller, J., 2002. Queuing or sharing? A critical evaluation of the single-bottleneck notion. *Cogn. Psychol.* 44, 193–251.
- Nelson, M.E., Bower, J.M., 1990. Brain maps and parallel computers. *Trends Neurosci.* 13, 403–408.
- Niaz, R.K., Beckmann, C.F., Iannetti, G.D., Brady, J.M., Smith, S.M., 2005. Removal of fMRI environment artifacts from EEG data using optimal basis sets. *Neuroimage* 28, 720–737.
- Pashler, H., 1994. Dual-task interference in simple tasks: data and theory. *Psychol. Bull.* 116, 220–244.
- Pashler, H., Johnston, J.C., 1989. Interference between temporally overlapping tasks: chromometric evidence for central postponement with or without response grouping. *Q. J. Exp. Psychol.* 41A, 19–45.
- Pashler, H.E., 1998. *The Psychology of Attention*. MIT Press, Cambridge, MA.
- Picton, T.W., 1992. The P300 wave of the human event-related potential. *J. Clin. Neurophysiol.* 9, 456–479.
- Quiroga, Q., Garcia, H., 2003. Single-trial event-related potentials with wavelet denoising. *Clin. Neurophysiol.* 114, 376–390.
- Rockstroh, B., Mueller, M., Cohen, R., Elbert, T., 1992. Probing the functional brain state during P300-evocation. *J. Psychophysiol.* 6, 175–184.
- Sackur, J., Naccache, L., Pradat-Diehl, P., Azouvi, P., Mazevet, D., Katz, R., Cohen, L., Dehaene, S., 2008. Semantic processing of neglected numbers. *Cortex* 44, 673–682.
- Schubert, T., 2008. The central attentional limitation and executive control. *Front. Biosci.* 13, 3569–3580.
- Schubert, T., Fischer, R., Stelzel, C., 2008. Response activation in overlapping tasks and the response-selection bottleneck. *J. Exp. Psychol. Hum. Percept. Perform.* 34, 376–397.
- Schubert, T., Szameitat, A.J., 2003. Functional neuroanatomy of interference in overlapping dual tasks: an fMRI study. *Cogn. Brain Res.* 17, 733–746.

- Sergent, C., Baillet, S., Dehaene, S., 2005. Timing of the brain events underlying access to consciousness during the attentional blink. *Nat. Neurosci.* 8, 1391–1400.
- Sigman, M., Dehaene, S., 2005. Parsing a cognitive task: a characterization of the mind's bottleneck. *PLoS Biol.* 3, e37.
- Sigman, M., Dehaene, S., 2006. Dynamics of the central bottleneck: dual-task and task uncertainty. *PLoS Biol.* 4, e220.
- Sigman, M., Dehaene, S., 2008. Brain mechanisms of serial and parallel processing during dual-task performance. *J. Neurosci.* 28, 7585–7598.
- Sigman, M., Jobert, A., Le Bihan, D., Dehaene, S., 2007. Parsing a sequence of brain activations at psychological times using fMRI. *Neuroimage* 35, 655–668.
- Strobel, A., Debener, S., Sorger, B., Peters, J.C., Kranczioch, C., Hoehstetter, K., Engel, A.K., Brocke, B., Goebel, R., 2008. Novelty and target processing during an auditory novelty oddball: a simultaneous event-related potential and functional magnetic resonance imaging study. *Neuroimage* 40, 869–883.
- Sutton, S., Braren, M., Zubin, J., John, E.R., 1965. Evoked-potential correlates of stimulus uncertainty. *Science* 150, 1187–1188.
- Szameitat, A.J., Lepsien, J., von Cramon, D.Y., Sterr, A., Schubert, T., 2006. Task-order coordination in dual-task performance and the lateral prefrontal cortex: an event-related fMRI study. *Psychol. Res.* 70, 541–552.
- Szameitat, A.J., Schubert, T., Muller, H.J., 2011. How to test for dual-task-specific effects in brain imaging studies—an evaluation of potential analysis methods. *Neuroimage* 54, 1765–1773.
- Telford, C.W., 1931. The refractory phase of voluntary and associative responses. *J. Exp. Psychol.* 14, 1–36.
- Tombu, M., Jolicoeur, P., 2003. A central capacity sharing model of dual-task performance. *J. Exp. Psychol. Hum. Percept. Perform.* 29, 3–18.
- Tootell, R.B., Reppas, J.B., Kwong, K.K., Malach, R., Born, R.T., Brady, T.J., Rosen, B.R., Belliveau, J.W., 1995. Functional analysis of human MT and related visual cortical areas using magnetic resonance imaging. *J. Neurosci.* 15, 3215–3230.
- Vanderperren, K., De Vos, M., Ramautar, J.R., Novitskiy, N., Mennes, M., Assecondi, S., Vanrumste, B., Stiers, P., Van den Bergh, B.R., Wagemans, J., Lagae, L., Sunaert, S., Van Huffel, S., 2010. Removal of BCG artifacts from EEG recordings inside the MR scanner: a comparison of methodological and validation-related aspects. *Neuroimage* 50, 920–934.
- Verleger, R., Jaskowski, P., Wascher, E., 2005. Evidence for an integrative role of P3b in linking reaction to perception. *J. Psychophysiol.* 19, 165–181.
- Viola, F.C., Thorne, J., Edmonds, B., Schneider, T., Eichele, T., Debener, S., 2009. Semi-automatic identification of independent components representing EEG artifact. *Clin. Neurophysiol.* 120, 868–877.
- Vogel, E.K., Luck, S.J., Shapiro, K.L., 1998. Electrophysiological evidence for a postperceptual locus of suppression during the attentional blink. *J. Exp. Psychol. Hum. Percept. Perform.* 24, 1656–1674.
- Warbrick, T., Mobascher, A., Brinkmeyer, J., Musso, F., Richter, N., Stoecker, T., Fink, G.R., Shah, N.J., Winterer, G., 2009. Single-trial P3 amplitude and latency informed event-related fMRI models yield different BOLD response patterns to a target detection task. *Neuroimage* 47, 1532–1544.
- Welford, A.T., 1952. The 'psychological refractory period' and the timing of high-speed performance — a review and a theory. *Br. J. Psychol.* 43, 2–19.
- Wong, K.F.E., 2002. The relationship between attentional blink and psychological refractory period. *J. Exp. Psychol. Hum. Percept. Perform.* 28, 54–71.
- Zylberberg, A., Slezak, D.F., Roelfsema, P.R., Dehaene, S., Sigman, M., 2010. The brain's router: a cortical network model of serial processing in the primate brain. *PLoS Comput. Biol.* 6, e1000765.